Express Polymer Letters Vol.18, No.8 (2024) 835–850
Available online at www.expresspolymlett.com
https://doi.org/10.3144/expresspolymlett.2024.62

Research article

Modified poly(ε-caprolactone) with larvae protein environmentally friendly nanofiber: Assessment of interface properties and characterization

Chin-San Wu[1*], *Shan-Shue Wang*[1], *Dung-Yi Wu*[2], *Wanwen Gu*[3]

[1]Department of Applied Cosmetology and Health Care, Taiwan Steel University of Science and Technology, 82101 Kaohsiung City, Taiwan, Republic of China
[2]Department of Materials Science and Engineering, Johns Hopkins University, Baltimore, MD 21218, USA
[3]Department of Statistic and Data, Cornell University, 14850 Ithaca, NY, USA

Received 11 April 2024; accepted in revised form 31 May 2024

Abstract. The protein from black soldier fly larvae was used as a functional ingredient of a novel green nanofiber. Larvae protein powder (LP) was blended with biodegradable poly(ε-caprolactone) (PCL) and processed in an electrospinning machine using a coaxial feeding/mixing method to produce nanofibers approximately 100–350 nm in diameter. To improve the dispersion and interface bonding of various PCL/LP nanofiber components, a homemade compatibilizer, maleic anhydride-grafted poly(ε-caprolactone) (MPCL), was added to form MPCL/LP nanofibers. The structure, morphology, mechanical properties, water absorption, cytocompatibility, wound healing, and biodegradability of PCL/LP and MPCL/LP nanofiber mats were investigated. The results showed enhanced adhesion in the MPCL/LP nanofiber mats compared to PCL/LP nanofiber mats; additionally, the MPCL/LP nanofibers exhibited increases of approximately 0.7–2.2 MPa in breaking strength and 9.0–22.8 MPa in Young's modulus. Decomposition tests using a simulated body fluid revealed that the addition of LP enhanced the decomposition rate of both PCL/LP and MPCL/LP nanofiber mats and *in vitro* protein release. Cell proliferation and migration analysis indicated that PCL, MPCL, and their composites were biocompatible for fibroblast (FB) growth. Biodegradability was tested in a 30 day soil test. When the LP content was 20 wt%, the degradation rate exceeded 50%.

Keywords: *cytocompatibility, wound healing activity, black soldier fly larvae protein, nanofiber, polycaprolactone*

1. Introduction

The depletion of global natural resources has become a pressing issue, bringing the critical topics of alternative resources and recycling resources to the forefront. To address the economic and environmental challenges, the use of black soldier fly (BSF) insects has been proposed [1–3]. These insects can consume organic waste materials from nature, such as kitchen waste, spoiled fruits, expired grains, and food processing byproducts. During the BSF larval stage, which lasts approximately 45–60 days, enzymes produced either by the larvae themselves or by symbiotic microorganisms break down complex macromolecules into smaller molecules. This biological process serves as a means of bioremediation, generating environmentally friendly and valuable materials for recycling within an ecological circular economy [4, 5].

BSF insects thrive in various environmental conditions, including tropical, subtropical, and temperate regions and can be cultivated on a mass scale [6–9]. They are also one of the primary insects utilized currently in large-scale insect farming for resource recycling. BSF larvae are rich in nutrients such as proteins

*Corresponding author, e-mail: t50008@tsust.edu.tw

and polyunsaturated fatty acids, making them a high-quality source of animal protein feed [10, 11]. The dry matter of larvae typically contains 30–53% protein, 20–41% fat, 20–41% chitin, and 2–9% other substances [12, 13]. These proteins have a complete amino acid composition that includes essential and non-essential amino acids, mainly as lysine, threonine, valine, histidine, and tyrosine [14–16], and provide good nutrients for skin, muscle, hair and nail formation [17, 18].

However, with the protein requirements for biodegradable polymer materials and technological advancements in this area, there is an increasing demand for proteins with enhanced properties and characteristics, especially in terms of their mechanical properties, processability, porosity, and pore size [19–21]. Electrospinning technology provides the means to meet these demands. This technique involves combining proteins with biodegradable polymers to form a solution that is then subjected to a high-voltage electric field. Under the influence of the electric field, the polymer molecules become charged, leading to their stretching and solidification into nanofibers [22–24]. Nanofiber mats produced in this manner exhibit excellent properties, such as breathability, moisture permeability, high surface area, and porosity [25, 26]. As such, these mats are suitable for use in wound dressings, drug delivery systems, and tissue engineering scaffolds in biomedically engineered materials.

There has been much interest recently in using electrospinning to manufacture fiber/s containing proteins. Suarato *et al*. [27] extracted keratin from wool and used keratin and polyvinylpyrrolidone to produce composite fibers for artificial scaffolds by electrospinning. These scaffolds could potentially be used to regulate the growth of skin tissue in the future. Flores-Nieves *et al*. [28] extracted casein from milk and used casein and polyethylene oxide, crosslinked by tannic acid, to fabricate fibers by electrospinning. They successfully obtained casein fibers with excellent mechanical properties and antibacterial activity, offering an innovative approach for functional textiles.

Polycaprolactone (PCL) is one of the most prominent biodegradable polyesters due to its excellent cytocompatibility, biodegradability, ductility, and low melting point [29–32]. The protein component in biodegradable materials should enhance the cytocompatibility and functionality of the materials, and increase the use of materials in the field of bioengineering. In this study, we developed new composite fibers containing PCL and proteins extracted from BSF larvae using an electrospinning technique. The coaxial structure and core–shell feed approach at the spinneret resulted in a well-structured composite. The addition of PCL grafted with maleic anhydride enhanced the interfacial compatibility between the two components. The new nanofibers composed of PCL and BSF protein provide good production efficiency for use in wound repair applications and other related material markets.

2. Experimental section

2.1. Materials

PCL of CAPA 6800 grade, with a molecular weight of 80 000, was purchased from Solvay Chemicals Co., Ltd. (Green River, WY, USA). 3-(4,5-dimethylthiazol-2-yl)-2,5-diphenyltetrazolium bromide (MTT), minimum essential medium (MEM), methanol, phosphoric acid, propidium iodide (PI), Triton X-100, and phosphate-buffered saline (PBS) were obtained from Sigma–Aldrich (St. Louis, MO, USA). Bovine serum albumin (BSA) and Coomassie Brilliant Blue G250 were purchased from Gibco (Waltham, MA, USA). Black soldier fly larvae were provided by Yu-Lu Bio-Agriculture Co., Ltd. (Lukang, Changhua, Taiwan). PCL-*g*-MA (grafting percentage about 0.88 wt%) was formed by grafting PCL with maleic anhydride (MA) [33]. PCL-*g*-MA (at 10%) was then mixed with PCL to make MPCL.

2.2. Preparation of protein from BSF larvae

First, the surface of BSF larvae was washed with clean water to remove soil and impurities, followed by spraying with 75% alcohol and exposure to ultraviolet light for 1 h for sterilization. Then, 50 g of black soldier fly larvae was crushed in a juicer with an appropriate amount of deionized (DI) water for 5 min. The whole BSF larvae extract was transferred to an ultrasonic oscillator and treated with proteinase (activity: 2.4 AU/g) for 2 h. The mixture was then heated to 90 °C for 10 min to deactivate the proteinase, followed by an adjustment of the pH to 7.0 with a buffer solution.

After heating to 40 °C to stabilize the viscosity of the protein, the mixture was centrifuged at 4800 g for 15 min to generate a three-layer mixture (soluble protein on the upper layer, oil in the middle layer, and insoluble protein precipitate on the bottom layer).

After the liquid layer was removed, a solution containing a magnetic stirrer and *n*-hexane (solid-liquid ratio of 1:5) was added to the residual and stirred at 250 rpm for 2 h to absorb the oil from the insoluble protein. The insoluble protein was obtained on filter paper by vacuum filtration, washed several times with ultrapure water, and placed in a fume hood for 2 days until all residual solvents evaporated completely.

2.3. Preparation of electrospinning solution and nanofiber mat

Preparation of BSF protein electrospinning solution A: BSF protein (10 g) was dissolved in a methanoic acid solvent in a 250 mL round-bottom flask to a final volume of 200 mL. The mixture was stirred at 250 rpm for 2 h until the BSF protein had dissolved completely to generate BSF protein electrospinning solution A.

Preparation of PCL electrospinning solution B: PCL or MPCL pellets (20 g) were dissolved in dichloromethane solvent in a 250 mL round-bottom flask to a final volume of 200 mL. The mixture was stirred at 350 rpm for 8 h until the pellets had dissolved completely into dichloromethane to generate PCL electrospinning solution B.

Solutions A and B were injected separately into syringes before entering the spinneret. The flow rate was controlled using an injection pump controller (Cole-Parmer/Antylia Scientific, Vernon Hills, IL, USA). The BSF protein electrospinning solution A was connected to the secondary flow rate end of the machine nozzle using a homemade coaxial spinneret, while the other end was connected to the PCL electrospinning solution B at the main flow rate end of the machine nozzle. The mixture was then electrospun by applying high voltage from a high-voltage power supply (FES-COS, Falco Tech Enterprise Co. Ltd. Taiwan) to the spinneret.

In the electrospinning process, the positive voltage was controlled at 24 kV, and the flow rates were set to 0.5 mL/h (secondary flow rate) and 0.9 mL/h (main flow rate) to ensure suitable processing conditions for the sample solution. The nanofibers were collected on an aluminum rotary collector (diameter: 10 cm; width: 20 cm) rotating at 50 rpm. The electrospinning process in the cone-jet mode allowed for continuous spinning for several hours, producing mats with a length of 10 cm and a width of 5 cm. The mats were then dried in an oven at 45 °C for 1 day and used to prepare standard specimens for various property identifications. The manufacturing process

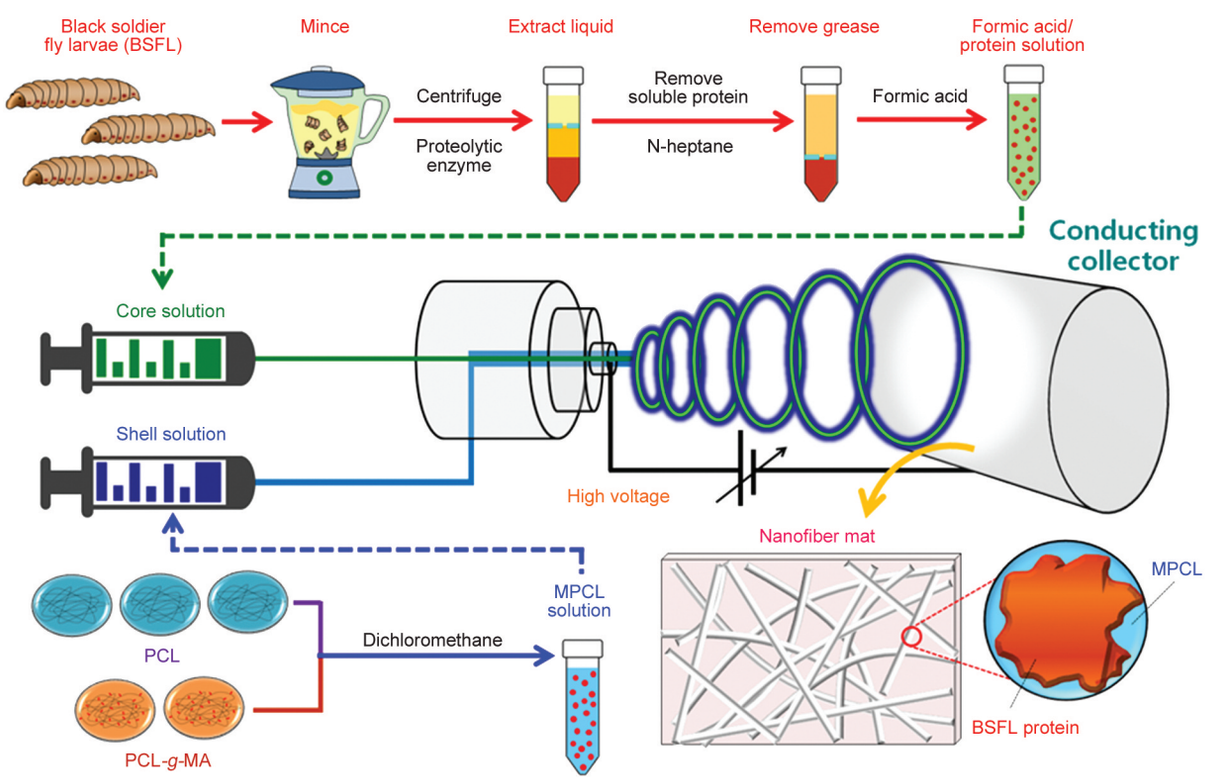

Figure 1. Fabrication of electrospun electrospinning solution and nanofiber mat from poly(ε-caprolactone) (PCL) and *Black Soldier Fly* larvae protein powder (LP).

Table 1. Formulation composites support designations and compositions.

Sample code	Component		
	PCL [wt%]	PCL-*g*-MA [phr]	LP [wt%]
PCL	100	–	–
PCL/LP 5wt%	95	–	5
PCL/ LP 10wt%	90	–	10
PCL/ LP 15wt%	85	–	15
PCL/ LP 20wt%	80	–	20
MPCL	100	10	–
MPCL/ LP 5wt%	95	10	5
MPCL/ LP 10wt%	90	10	10
MPCL/ LP 15wt%	85	10	15
MPCL/ LP 20wt%	80	10	20

PCL: polycaprolactone;
MPBSL: modified PCL [(added compatibility maleic anhydride (MA) grafted PCL (PCL-*g*-MA)];
LP: larvae protein powder.

is described in Figure 1, and the composition formula is shown in Table 1.

2.4. Surface hydrophilicity and cytocompatibility measurements

2.4.1. Surfaces hydrophilicity evaluation

The hydrophilicity of PCL/LP and MPCL/LP nanofiber mats was evaluated using a contact angle goniometer. Each type of nanofiber mat (50×35×0.06 mm) was placed in a vacuum oven at 45±1 °C until it reached a constant weight, serving as samples for the hydrophilicity evaluation. Then, 3 µL of DI water droplets were dropped onto the nanofiber mat, and the surface contact angles (OCA50, Diethelm Keller Siber Hegner Co. Ltd., Taiwan) were recorded. The water droplets were attached to the nanofiber mat for 30 s. The average value from six measurements was recorded.

After drying, the weight of the nanofiber mat was measured. Subsequently, the nanofiber mat was placed in a 50 mL conical flask and immersed in 30 mL of distilled water. Samples were then taken out every 10 days until the 80th day. The surface water of the sample was wiped dry using clean paper towels, and the weight of the nanofiber mat was measured. The water absorption percentage (W_1%) was then calculated using the Equation (1), which provided the weight gain as a percent:

$$W_1\% = \frac{W_b - W_a}{W_a} \cdot 100\% \quad (1)$$

where W_a: the weight of the dry samples was measured and recorded, W_b: after withdrawing a sample from the water, surface moisture was removed using clean paper, and the film mass was measured and recorded.

2.4.2. Cytocompatibility analysis

The CCD-966SK FBs (BCRC 60153) from the Bioresource Collection and Research Center (Taiwan) were cultured in a growth medium until reaching a stable growth state. Then, $2 \cdot 10^5$ cells were seeded into each well of 24 well plates containing PCL, MPCL, or their composite mat. The cells were cultured at 37 °C with 5% CO_2. MTT analysis was performed. Then, 0.1 mL/well of MTT reagent was added to the culture medium and allowed to incubate for 5 h. After incubation, 0.1 mL of dimethyl sulfoxide (DMSO) was added, and the mixture was shaken for 6 min. The absorbance was measured at a wavelength of 540 nm using an enzyme-linked immunosorbent assay (ELISA) in a 96 well plate to determine the cell proliferation.

To assess the effect of various mat samples on the cell cycle of cell lines, flow cytometry (FACSCalibur, Becton Dickinson, Franklin Lakes, NJ, USA) was used with PI staining to evaluate the distribution of the cell cycle. Each $1 \cdot 10^5$ CCD-966SK cell was seeded into a 6 cm culture dish containing various PCL or MPCL composite mat samples separately and sterilized under ultraviolet light for 1 h. The control was without a mat sample. After 1 day of culture, the cells were fixed with 70% ethanol for 8 h, and stained with PI/Triton X-100 DNA staining solution. After incubating at room temperature in the dark for 30 min, flow cytometry was used to analyze $1 \cdot 10^5$ cells using the FL2 PMT parameter, and the data were analyzed using WinMDI 2.9 software (Microsoft Corp., Redmond, WA, USA).

To observe the changes in nuclear morphology of CCD-966SK cells and the effect of various mat samples on the cell cycle of cell lines, flow cytometry (FACSCalibur, Becton Dickinson, Franklin Lakes, NJ, USA) was used with PI staining to evaluate the distribution of the cell cycle.

To observe the effect of various mat samples on nuclear morphology change of CCD-966SK cells, fluorescence microscopy was applied. The CCD-966SK cells were prepared as described above. After 1 day of culture, the cells were fixed with 4% paraformaldehyde at room temperature for 30 min, rinsed with

PBS, added DAPI and reacted for 30 min, and then observed the changes in the nuclear morphology of CCD-966SK cells through a 330–380 nm fluorescence microscope.

For wound healing assays, $4 \cdot 10^4$ CCD-966SK cells were cultured in 6 cm culture dishes for 1 day. After scratch wounds were created using sterile forceps, the nanofiber mats were fixed onto the wounds and cultured for 1 day. The nanofiber mats were then removed, and fresh culture medium was added for another day of culture. The migration of cells into the gap area was observed using a microscope, and the remaining wound area was determined using ImageJ software (National Institutes of Health, Bethesda, MD, USA).

2.5. Instrumentation

PCL or MPCL and their composite samples were analyzed using Fourier-transform infrared spectroscopy (FTIR, PerkinElmer, Waltham, MA, USA) to determine the structural information based on the absorption peaks. The resolution was set to 4 cm^{-1}, and the scan range was from 420 to 4000 cm^{-1}. X-ray diffraction (XRD; D2 PHASER, Bruker, Mannheim, Germany) was employed to analyze the crystalline structure of the samples using Cu-Kα radiation. The conditions for analysis were set at 40 kV, 25 mA, a scanning rate of 2°/min, and a scanning angle range of 10° to 60°. X-ray photoelectron spectroscopy (XPS, PHI 5000, Ulvac-phi Inc., Kanagawa, Japan) was utilized to examine the structure of various samples. Tensile properties were determined using a universal testing machine (HT-9102; Hung Ta Machines Co., Ltd., Taichung, Taiwan) following ASTM D638 Type IV standard specifications. The tests were conducted at a crosshead speed of 2 mm/min, and data were obtained by repeating the test at least five times and averaging the results. The surface morphology of the samples was examined using scanning electron microscopy (SEM; Hitachi S-4800; Tokyo, Japan). PCL, MPCL, and their composite samples were coated with a gold layer using a sputterer at 20 kV for 150 s to increase conductivity. The coated samples were then examined using the SEM apparatus.

2.6. Phosphate-buffered saline *in vitro* degradation test

Each sample from a different series was weighted as initial weight, then immersed into a 125 mL beaker containing 60 mL of 1× PBS. The beakers were then covered with aluminum foil and left at room temperature. After 10, 20, 30, 40, and 50 days, the samples were removed, the surface moisture of the samples was removed, and the samples were dried to a constant weight as the residual weight. Degraded weight was calculated by subtracting the residual weight from the initial weight. The *in vitro* degradation performance was evaluated as the weight ratio which was the degraded weight/initial weight.

2.7. Protein content testing

The solutions obtained from the above *in vitro* degradation tests were subjected to centrifugation at 3600 rpm. Two-thirds of the upper liquid layer was then removed, and the remaining solution was thoroughly mixed using a test tube shaker. A volume of 30 μL from each mixture (degradation solution) was taken and mixed with 1.5 mL of Coomassie Brilliant Blue G250 using a test tube shaker. After 5 min of incubation, the protein content release results were analyzed using ELISA at a wavelength of 595 nm.

2.8. Environmentally biodegradability assessment

Samples of various nanofiber mats were cut into dimensions of 35×25×0.05 mm. The samples were buried at a depth of 10–15 cm underground in agricultural land with 50–60% moisture content located in Luzhu District, Kaohsiung City, Taiwan.

Every 5 days, the samples were removed from the soil to observe the degradation of the nanofiber mats. The degradation loss rate was calculated, and an analysis of the surface degradation structure was conducted over a period of 30 days.

2.9. Statistical analysis

The experimental data were analyzed using analysis of variance (ANOVA). Mean values are given as the mean ± standard deviation. Differences were considered significant when $p < 0.05$. The analysis was conducted using SPSS software, and the experimental data were averaged from five repetitions.

3. Results and discussion

3.1. Nanofiber structure analysis

FTIR, XPS, and XRD spectra were used to investigate PCL, MPCL, and composite nanofibers to understand the structural composition of the nanofibers. From a comparison of FTIR spectra shown in

Figure 2 curves (a) and Figure 2 curves (b), the common absorption peaks of PCL appeared at 1700–1760 and 500–1500 cm^{-1}. PCL-*g*-MA was present as two additional absorption peaks at 1785 and 1853 cm^{-1} that were attributed to the characteristic peaks formed by the maleic anhydride functional group in the added MA for compatibility [34]. Compared to PCL (Figure 2 curve (a)), the PCL/LP nanocomposite fibers (Figure 2 curve (c) showed three new peaks at 3296 cm^{-1} corresponding to amide groups (amide, NH stretching), 1647 cm^{-1} (amide I, C=O stretching), and 1543 cm^{-1} (amide II, NH bending), coinciding with the effect of LP in PCL/LP nanofibers [35]. Additionally, in the comparison of PCL/LP (Figure 2 curve (c)) and MPCL/LP (Figure 2 curve (d)), besides the common absorption peak of LP and PCL, a new absorption peak at 1738 cm^{-1} was observed, as shown in Figure 2 curve (d) that is associated with the formation of ester bonding between LP and MPCL [36]. In the comparison of PCL/LP (Figure 2 curve c)) and MPCL/LP (Figure 2 curve (d)), the peak at 3296 cm^{-1} shifted to 3217 cm^{-1}, possibly due to the phenomenon of hetero-associated hydrogen bonds between MPCL and LP [37].

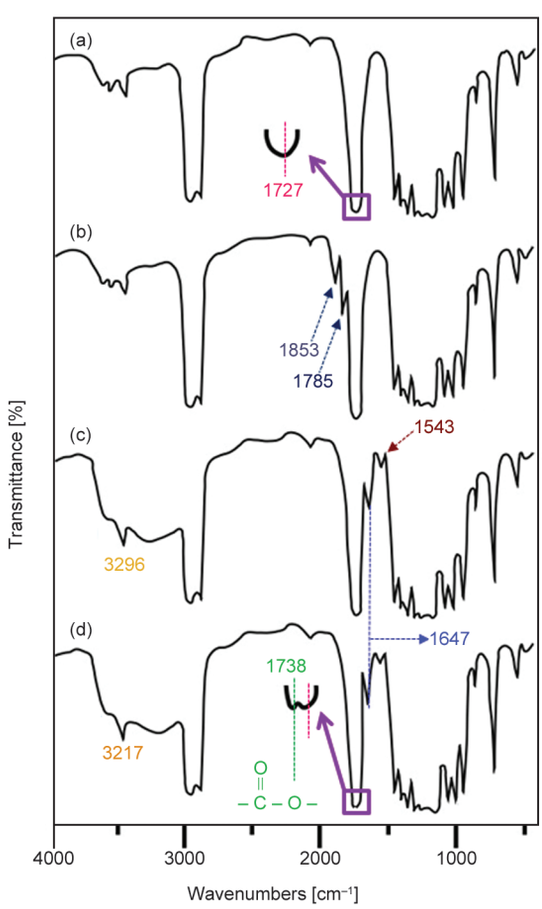

Figure 2. Fourier-transform infrared spectra of curve (a) poly (ε-caprolactone) (PCL), curve (b) maleic anhydride-grafted PCL (MPCL), curve (c) PCL/larvae protein powder (LP) (10 wt%), and curve (d) MPCL/LP (10 wt%).

Figure 3a depicts the spectrum of pure PCL, showing the electron emission positions of carbon (C 1s, 280–291 eV) and oxygen (O 1s, 533–534 eV) [38]. However, in a comparison between Figure 3a and Figure 3b, a new peak at 289.5 eV [O–C=O, C 1s] was observed in MPCL, which was attributed to the presence of MA-containing material in the compatibilizer added in MPCL [39]. When comparing PCL/LP and MPCL/LP nanocomposite fibers (Figure 3c and Figure 3d) to PCL (Figure 3a), two new peaks were identified at 285.8 eV [N–C, C 1s] and 399.9 eV [N 1s], respectively. These peaks are associated with the presence of proteinaceous components resulting from the addition of LP to PCL or MPCL [40].

Figure 4 shows the X-ray diffraction patterns of PCL, PCL/LP (10 wt%), MPCL/LP (10 wt%), and LP nanocomposite fibers. Pure PCL exhibited two peaks at 21.7° (1) and 23.6° (2), consistent with previous reports (Figure 4 curve (a)) [41]. PCL/LP nanocomposite fibers displayed an additional absorption peak at 20.7° (Figure 4 curve (b)), attributed to the LP structure, as shown in Figure 3 curve (d) [42]. Compared to PCL/LP (Figure 4 curve (b)) and MPCL/LP (Figure 4 curve (c)), we observed that besides the common absorption peaks of LP and PCL, a new absorption peak appeared at 18.1° (Figure 4 curve (c)) from the ester groups that formed due to the reaction between MA in LP and MPCL [43].

3.2. Morphology and tensile properties analysis

According to the SEM micrograph and average diameter distribution data analysis in Figure 5, the average fiber diameter increases as the LP content ratio increases. Figure 5a–5c shows that PCL/LP 0, 10 and 20 wt% are 136±23, 263±31 and 341±35 nm respectively. Compared with PCL/LP 0 wt%, when LP is increased by 20 wt%, the average fiber diameter increases by about 200 nm; The average fiber diameter also increases after adding LP to MPLC. The MPLC, MCL/LP 10 and 20 wt% have 143±25, 219±27, and 309±28 nm, respectively (Figure 5d–5f). However, the average diameter of MPCL/LP (10 and 20 wt%) nanofiber mats is about 32–44 nm smaller than that of PCL/LP (10 and

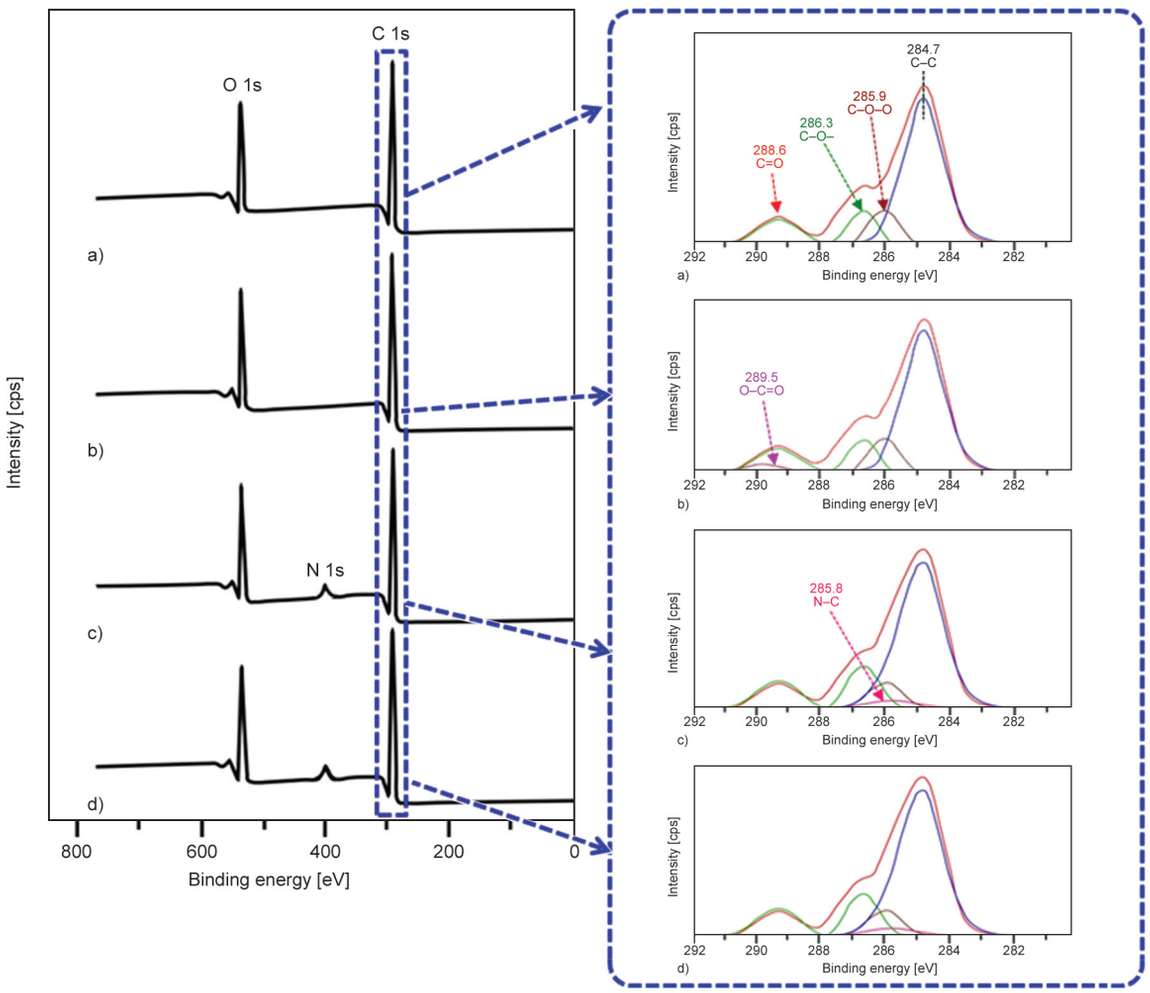

Figure 3. X-ray photoelectron spectroscopy survey spectrum of a) PCL, b) MPCL, c) PCL/LP (10 wt%), and d) MPCL/LP (10 wt%).

and 20 wt%) nanofiber mats; while MPCL/LP can provide thinner average diameter, which is mainly attributed to the formation of chemical bonds between MPCL and LP, leading to an increase in their interfacial adhesion.

Composite materials can be used to cover wounds and protect them during the wound healing process. Therefore, the mechanical properties of composite materials are important. Figure 5i and Table 2 show the stress–strain curves, Young's modulus, tensile strength, and elongation at break of the composite. The tensile strength/Young's modulus of MPCL nanofiber mats (3.26±0.16/36.8±5.2 MPa) was slightly lower than that of pure PCL (3.35±0.13/37.6±5.1 MPa) due to the addition of a compatibilizer, which leads to a looser molecular structure and slight reductions in Young's modulus and the tensile strength. However, with increasing LP content in PCL, Young's modulus and the tensile strength of PCL/LP nanofiber mat samples decreased significantly from 3.35±0.13/37.6±5.1 MPa to 1.61±0.18/20.3±6.2 MPa, possibly due to poorer adhesion to the PCL matrix with increasing LP content. In contrast, in MPCL/LP samples, Young's modulus and tensile strength increased with the LP content due to the better encapsulation of LP by MPCL and improved interfacial adhesion. In summary, Young's modulus and the tensile strength of MPCL/LP were approximately 9.0–22.8 MPa and 0.7–2.2 higher respectively than those of PCL/LP. However, when the LP content in MPCL/LP samples increased from 10 to 20%, Young's modulus and the tensile strength decreased slightly due to the excessive adhesion of MPCL to LP. This led to aggregation and a further reduction in Young's modulus and tensile strength, as well as uneven fibers, as shown in Figure 5c and Figure 5f.

The elongation at break (ε) values of PCL/LP and MPCL/LP nanofiber mats decreased with increasing LP content, as shown in Table 2; however, the elongation at break of MPCL/LP nanofiber mats was

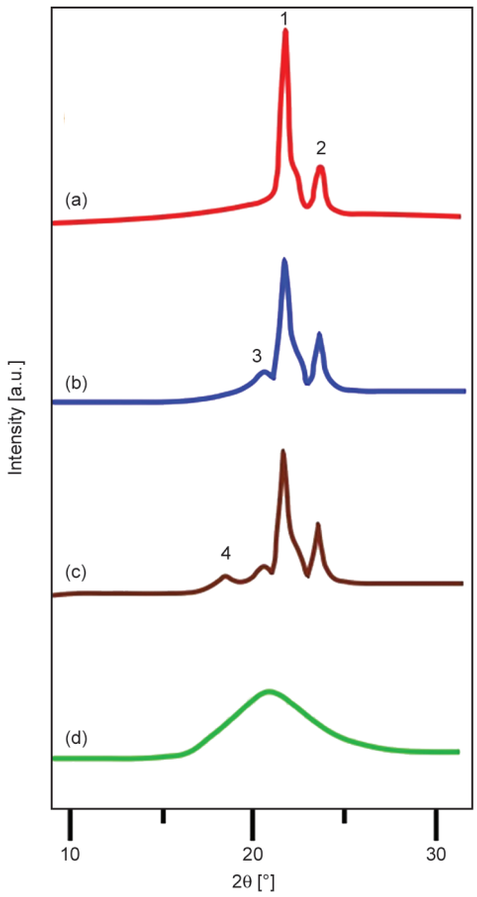

Figure 4. X-ray diffraction spectra: curve (a) PCL, curve (b) PCL/LP (10 wt%), curve (c) MPCL/LP (10 wt%), and curve (d) LP (10 wt%).

slightly higher than that of PCL/LP nanofiber mats due to better interfacial connectivity between MPCL and LP, indicating higher elongation at break for MPCL/LP nanofiber mats compared to PCL/LP nanofiber mats. Based on the above, the mechanical properties of MPCL/LP composite materials have been improved, which can further help patients reduce flexibility and discomfort during exercise and provide better protection.

3.3. Hydrophilic properties and cytocompatibility analysis

To assess the surface wettability of PCL/LP and MPCL/LP samples, contact angle and water absorption tests were conducted and analyzed. From the contact angle measurements shown in Figure 6a, the contact angles of PCL and MPCL samples were 88.44±1.71° and 87.61±2.05°, respectively. However, upon addition of 10 and 20 wt% LP to PCL/LP samples, the contact angles decreased to 82.39±3.28° and 75.83±4.57°, respectively. The reduction in contact angle was attributed to the presence of LP, which intervenes in the structure of PCL and MPCL, causing pore formation that allows water penetration. Additionally, for PCL/LP and MPCL/LP samples with the same LP content, the hydrophilicity of PCL/LP was higher than that of MPCL/LP (Figure 6a). This is because the bonding between MPCL and LP reduced its permeability and enhanced its hydrophobicity [44].

Figure 6b shows the water absorption of PCL/LP and MPCL/LP samples when immersed in water. For pure PCL, the water absorption increased at a slow rate. However, in samples containing LP, the water absorption increased with the LP content. This phenomenon is attributed to the influence of LP on the structure of PCL and MPCL, leading to higher water absorption in PCL/LP and MPCL/LP samples compared to pure PCL samples. Furthermore, it is noted that the water absorption of MPCL/LP was lower than that of PCL/LP. This is because chemical bonds form between MPCL and LP, resulting in better encapsulation of LP by MPCL and enhanced water resistance. Therefore, the main reason for the decrease in water absorption is the improved water resistance due to the bonding between MPCL and LP.

Figure 6c shows the cytocompatibility of PCL, PCL/LP, and MPCL/LP nanocomposite fibers evaluated using the CCD-966SK FB cell growth vitality assay. The nanofiber mats were cultured with CCD-966SK FBs cells for 1, 3, and 7 days, and the cell growth vitality was assessed using an MTT assay. The results indicated that on the first day, the cell viability of the control group and the other samples showed no significant difference. However, on the third and seventh days, a noticeable increase in cell viability was observed in the PCL/LP and MPCL/LP samples. This increase is primarily attributed to the rich nutritional content of LP, which contains various components such as free amino acids as cysteine, tryptophan, histidine, or tyrosine, dipeptides, tripeptides, *etc*. [45], providing CCD-966SK cells with the necessary nutrients for absorption and cell proliferation. Therefore, the application of nanofiber mat products did not show toxic effects, indicating that they have good cytocompatibility.

In Figure 6d and Figure 6e, during the replication and division processes, cells exhibited changes in DNA, reflecting the cell count. The first peak of absorption (G1) coincides with the DNA growth phase, the second peak indicates the mitotic phase (G2/M), and the peak between G1 and G2/M represents the

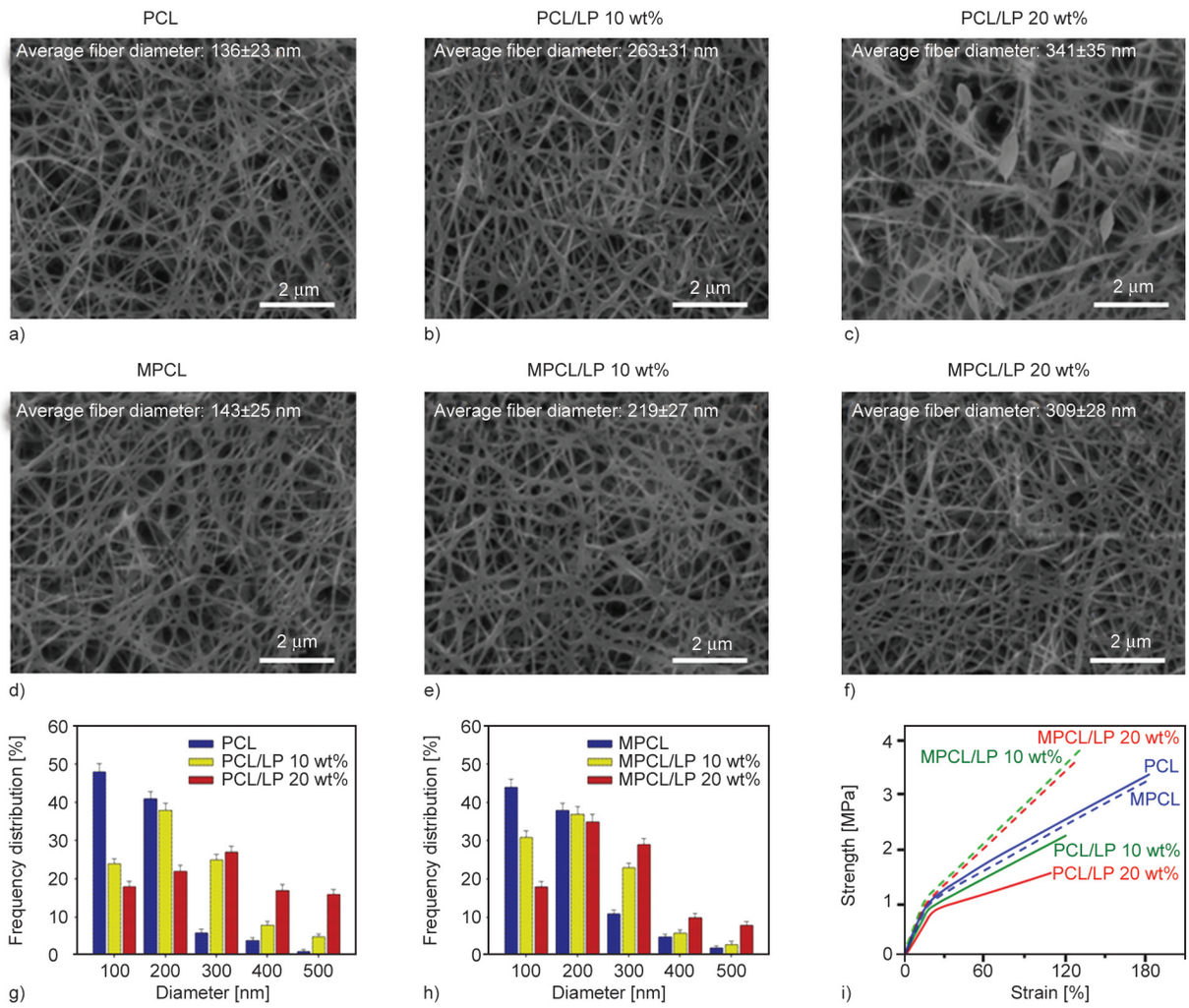

Figure 5. Scanning electron microscopy images of the distribution of a) PCL, b) PCL/LP (10 wt%), c) PCL/LP (20 wt%), d) MPCL, e) MPCL/LP (10 wt%), and f) MPCL/LP (20 wt%). Frequency distribution *versus* diameter of PCL/LP (g) and MPCL/LP (h) series. i) Tensile properties of stress–strain curves of PCL, MPCL, PCL/LP and MPCL/LP nanofibers mats.

Table 2. Effects of larvae protein powder (LP) content on the tensile properties of polycaprolactone (PCL)/LP and modified PCL (MPCL)/LP nanofibers.

LP [wt%]	PCL/LP			MPCL/LP		
	E **[MPa]**	**δ [MPa]**	**ε [%]**	***E*** **[MPa]**	**δ [MPa]**	**ε [%]**
0	37.6±5.1	3.35±0.13	183.6±5.6	36.8±5.2	3.26±0.16	182.8±5.7
5	32.3±5.8	2.81±0.15	150.5±5.8	40.3±5.7	3.56±0.20	151.3±5.9
10	27.7±6.0	2.39±0.17	120.8±6.0	48.8±5.8	3.86±0.23	131.2±6.2
15	23.6±6.1	2.13±0.17	111.3±6.2	45.3±5.9	3.78±0.25	128.5±6.3
20	20.3±6.2	1.61±0.18	109.5±6.5	43.1±6.0	3.72±0.28	126.3±6.5

δ: tensile strength,
ε: elongation at failure,
E: Young's modulus.

DNA replication phase (S) [46]. The cell cycles of CCD-966SK FBs cells cultured with the Control group and various PCL/LP or MPCL/LP series nanofiber mats were examined. There were no significant differences ($p < 0.05$) in the absorption peaks of the G1, S, and G2/M regions, and there was only a slight change in the DNA content area, but the change was not significant ($p < 0.05$) in Figure 6d and Figure 6e. Based on the above results, it can be confirmed that different PCL/LP or MPCL/LP series nanofiber mats do not induce significant DNA changes in CCD-966SK cells.

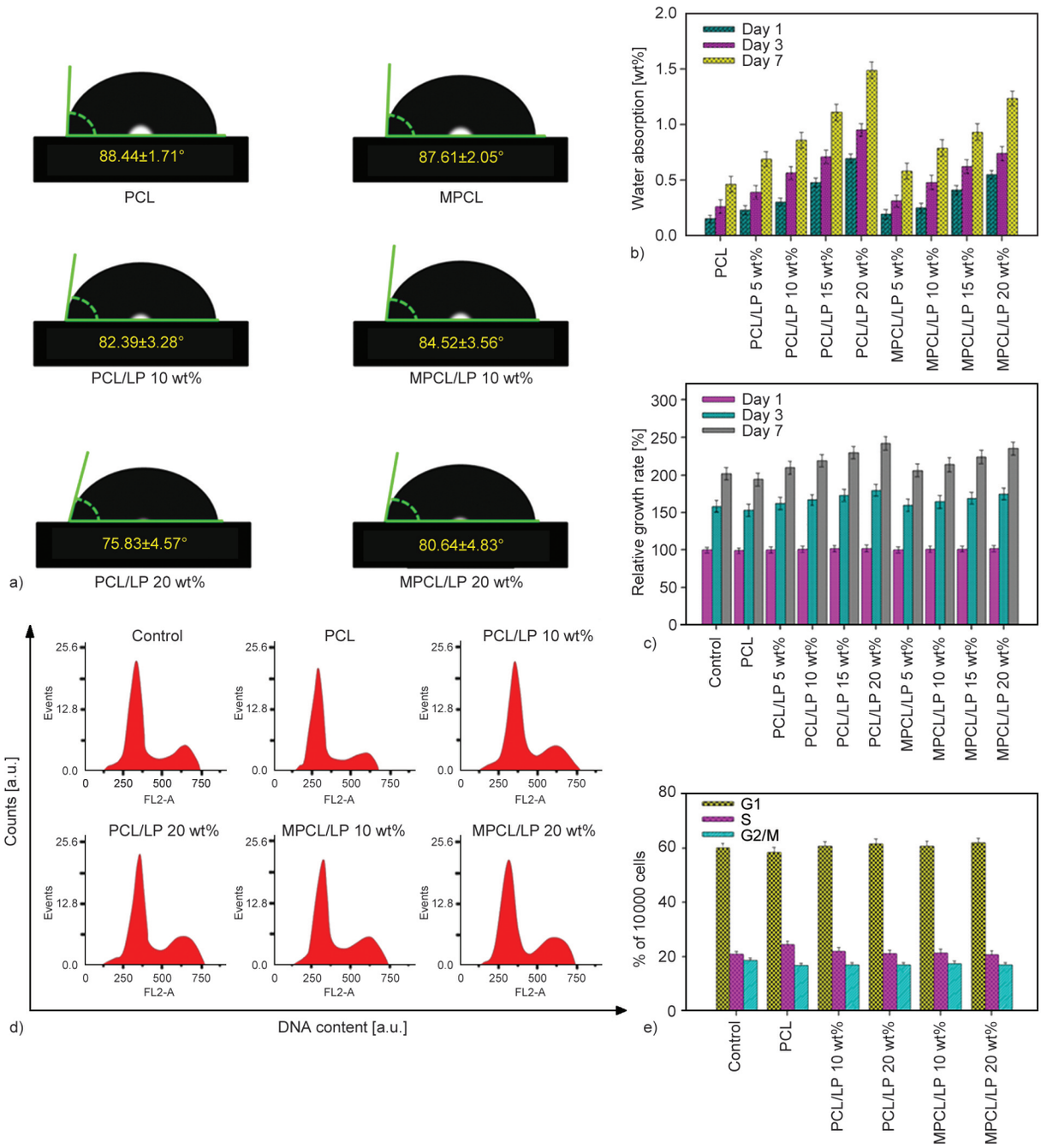

Figure 6. a) Water contact angles profile, b) water absorption, and c) 3-(4,5-dimethylthiazol-2-yl)-2,5-diphenyltetrazolium bromide (MTT) test evaluation of PCL, MPCL, PCL/LP, and MPCL/LP mats. d) Cell cycle of PCL, MPCL, and their composite membranes measured by flow cytometry; data plotted as cell numbers versus cell DNA content. e) Cell cycle histograms represent the percentage of the total cell population in different phases.

3.4. *In vitro* degradation assay and protein assessment

To simulate the *in vitro* degradation of the scaffolds, Figure 7a depicts the degradation behavior of different types of PCL/LP or MPCL/LP series mats placed in PBS. Weight loss due to degradation of PCL/LP or MPCL/LP series mats increased with the soaking time in PBS buffer. Furthermore, the magnitude of weight loss followed the order PCL/LP > MPBCL/LP > PCL or MPCL, indicating that the degradation rate of PCL/LP or MPCL/LP series nanofiber mats was higher than that of the original PCL. More pores and/or loose structure formations were created in PCL/LP and MPCL/LP after LP was incorporated into PCL or MPCL, respectively. The pores and more hydrophilic LP attract water molecules to the fibers,

thus accelerating the increase in weight loss. Additionally, MPCL/LP exhibited lower degradation weight loss compared to the PCL/LP series nanofiber mats, which can be attributed to the formation of bonds between LP and MPCL. Consequently, the MPCL/LP series nanofiber mats exhibited a slightly reduced degradation efficiency due to this improved bonding, resulting in a slight decrease in degradation performance.

The solution from *in vitro* degradation was taken for protein content testing. Figure 7b shows that the protein quantity of the *in vitro* degradation solution of

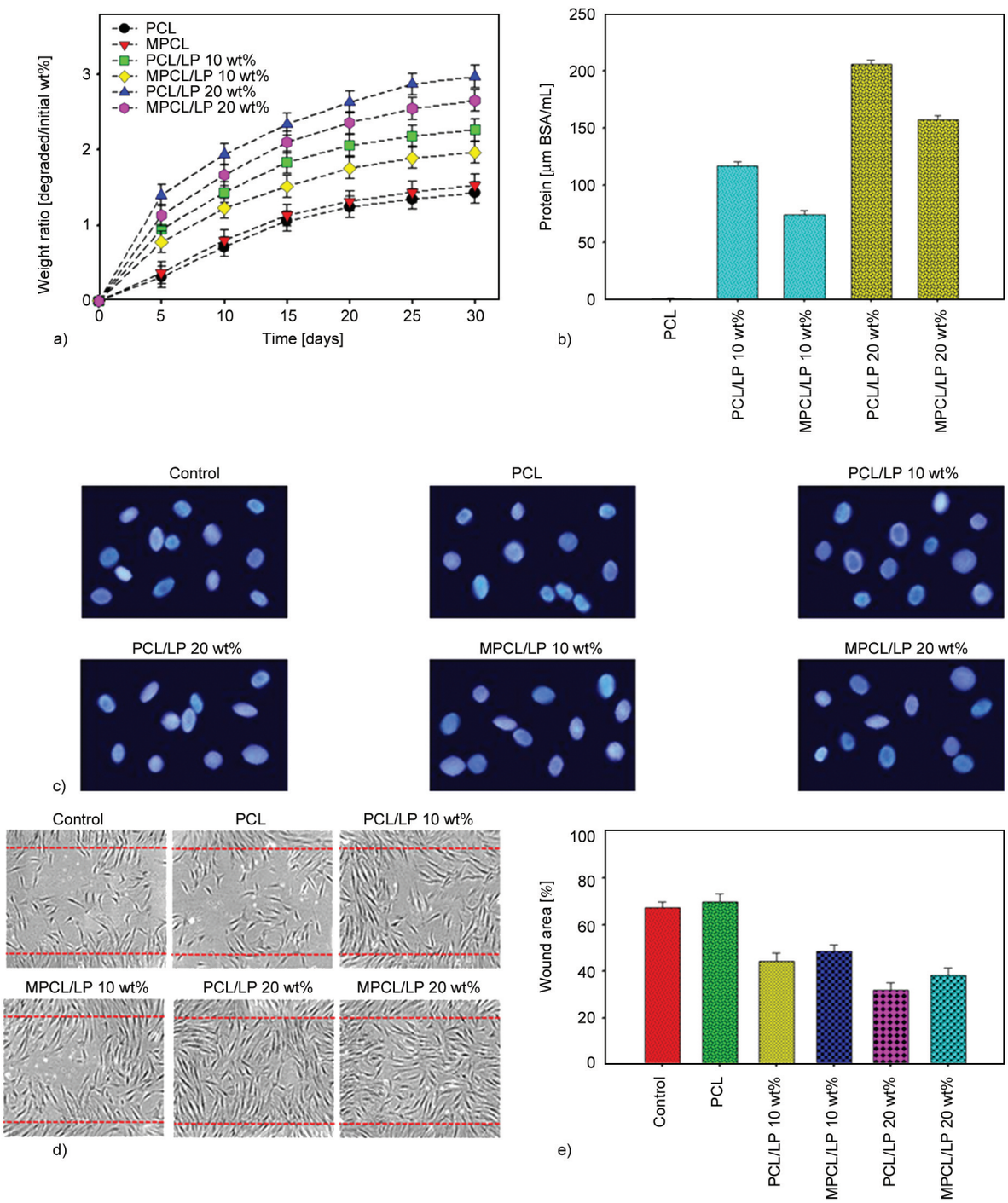

Figure 7. a) *In vitro* decomposition rate of PCL, MPCL, PCL/LP, and MPCL/LP mats in simulated body fluid buffer. b) Protein content of *in vitro* decomposition solution for PCL/LP and MPCL/LP series nanofiber mats. c) Nuclear morphology of CCD-966SK cells stained with DAPI under fluorescence microscope. d) Growth patterns of CCD-966SK fibroblasts by inverted microscopy after cells migrate into interstitial areas with different ratios of PCL/LP and MPCL/LP nanofibers for 1 day. e) Wound area histograms of control, PCL, PCL/LP, and MPCL/LP mats.

PCL/LP or MPCL/LP series nanofiber mats increased with the LP amount. This phenomenon occurs because LP contains proteins such as wheat protein and alcohol-soluble protein [47, 48]; thus, a higher LP content results in a higher protein content in the analysis. Additionally, the degradation protein content of MPCL/LP nanofiber mats was slightly lower than that of PCL/LP nanofiber mats. This is because the bonding between LP and MPCL leads to a smaller release of LP content within the nanofiber mats, consequently resulting in a decrease in protein content.

3.5. Nuclear morphology, cell migration and wound behavior test

In order to examine whether PCL, MPCL, PCL/LP, and MPCL/LP composite nanofiber mats affect cell growth, DAPI was used to perform fluorescent staining analysis on CCD-966SK cells co-cultured with composite nanofiber mats. According to the cell nucleus fluorescence image in Figure 7c, PCL, MPCL, PCL/LP, and MPCL/LP composite nanofiber mats do not affect the growth of skin cells.

To understand whether PCL/LP and MPCL/LP promote wound healing after cultivation, an *in vitro* cell migration assay was conducted to analyze the migration ability of FB cells influenced by the nanofiber mat. After culturing PCL/LP and MPCL/LP nanofiber mats with CCD-966SK for 24 h, Figure 7d shows that the migration speed of the Control and PCL was relatively slow, whereas there was an obvious migration increase in PCL/LP and MPCL/LP nanofiber mats. Furthermore, as shown in Figure 7e, the wound area of PCL/LP and MPCL/LP 10/20 wt% was reduced to 44.25±3.59%/32.09±3.19% and 48.51±2.88%/38.47±3.07%, respectively. This increase in the migration rate may be attributed to the proteins present in LP. Additionally, the wound area of MPCL/LP was slightly higher than that of PCL/LP, which could be due to the effective coverage provided by MPCL, preventing LP from being released effectively and thereby leading to a larger wound area [49].

3.6. Environmental biodegradation analysis

To enhance the degradation behavior of nanofibers after disposal, an assessment of their degradation under burial in soil was conducted, as illustrated in Figure 8. From Figure 8a, various types of nanofiber mats exhibited an increase in their biodegradation rate over time. Specifically, both PCL and MPCL showed a relatively stable and slowly increasing trend. However, in PCL/LP and MPCL/LP, a rapid increase in degradation was observed within the first 15 days. This phenomenon is attributed to the presence of LP within PCL and MPCL, which creates gaps in the structure, allowing soil microorganisms to invade and accelerate the degradation of the nanofiber mats.

After 15 days, the biodegradation rate began to slow as the internal less-stable structures were eroded away by soil-degrading microorganisms, leaving a more stable structure and thus slowing down the degradation. Additionally, Figure 8b shows that the deterioration of various nanofiber mats increased gradually with time. The degradation of PCL/LP was superior to that of MPCL/LP, primarily due to the better bonding effect between MPCL and LP. This improved bonding led to better coverage compared to PCL/LP, resulting in slightly lower degradation of MPCL/LP compared to PCL/LP.

According to the behavior of PCL, MPCL, PCL/LP, and MPCL/LP in PBS solution (Figure 7a) and soil (Figure 8a), PCL has a higher degradation effect than MPCL. This is because MPCL contains grafted maleic anhydride, resulting in a tighter structure than PCL. External moisture can more easily access and degrade PCL. Therefore, PCL showed a higher degradation effect than MPCL in terms of *in vitro* degradation and soil degradation; similarly, the degradation efficiency of PCL/LP was also higher than that of MPCL/LP, which can be attributed to the bonding reaction between MPCL and LP. This results in a tighter structure, which prevents external moisture from accessing the MPCL/LP.

4. Conclusions

This study focused on incorporating LP, derived from recycled insect larvae protein, with PCL to produce PCL/LP and MPCL/LP nanofiber mats via electrospinning. The manufacturing process, structure, tensile properties, cytocompatibility, wound healing, and degradation of PCL/LP and MPCL/LP nanofiber mats were investigated. FTIR, XPS, and XRD spectroscopic analyses indicated condensation reactions between MPCL and LP, resulting in enhanced adhesion and a more uniform diameter of MPCL/LP nanofiber compared to PCL/LP nanofiber. Moreover, the tensile strength at break and Young's modulus values of MPCL/LP were approximately 0.7–2.2 and 9.0–22.8 MPa higher than those of PCL/LP, respectively.

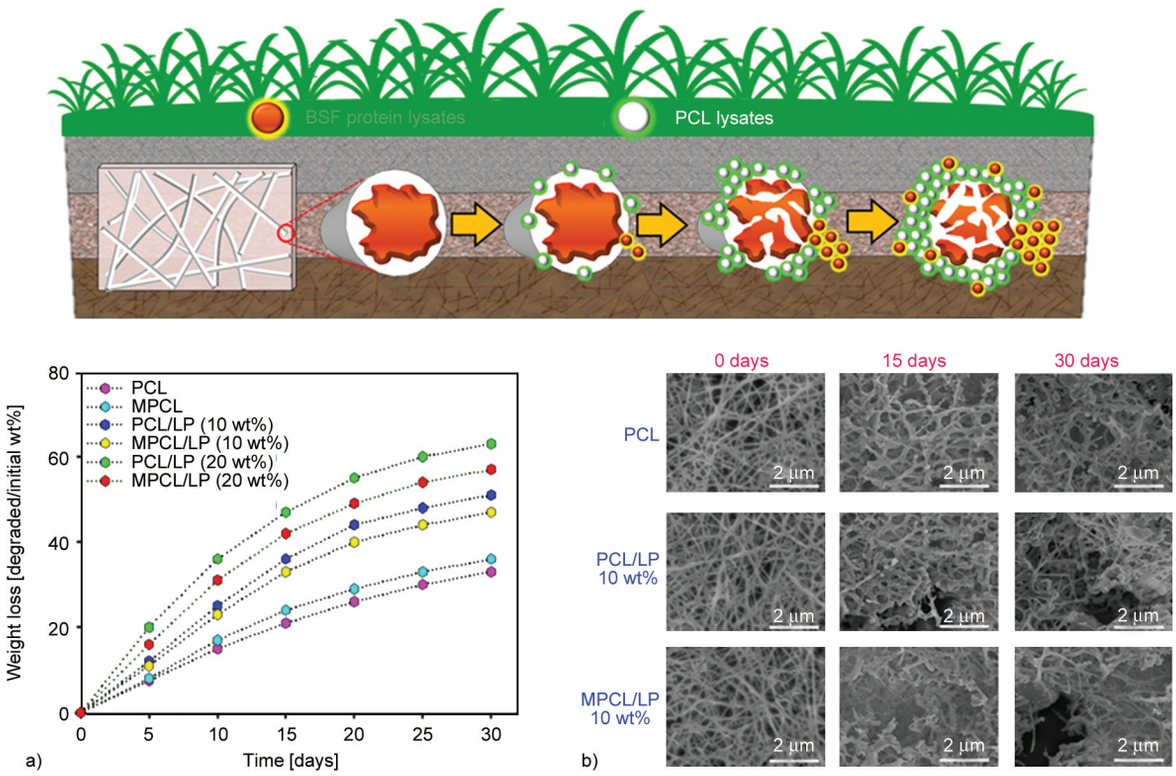

Figure 8. a) Biodegradability of PCL, MPCL, and their composite mats in soil. b) Scanning electron microscopy images of the morphology of PCL, PCL/LP (10 wt%) and MPCL/LP (10 wt%) mats as a function of incubation time (0,15 and 30 days) in soil.

Additionally, during the *in vitro* degradation process, the presence of LP in PCL/LP and MPCL/LP nanofiber mats led to enhanced degradation efficiency and protein release. Moreover, in cell viability and migration assays, PCL/LP and MPCL/LP nanofiber mats demonstrated excellent cytocompatibility and wound healing capabilities. Cell cycle analysis using CCD-966SK FBs showed no cell growth effect caused by PCL/LP and MPCL/LP nanofiber mats, indicating their potential for biomedical material applications. Thus, incorporating larval protein into PCL or MPCL substrates not only contributed to resource recycling but also enhanced the properties of mechanical strength, cytocompatibility, wound healing, and biodegradability of the nanofiber mats.

Acknowledgements

The author thanks the Ministry of Science and Technology (Taipei City, Taiwan, R.O.C.) for financial support (NSTC 112-2221-E-244-001-)

References

[1] Liu T., Klammsteiner T., Dregulo A. M., Kumar V., Zhou Y., Zhang Z., Awasthi M. K.: Black soldier fly larvae for organic manure recycling and its potential for a circular bioeconomy: A review. Science of the Total Environment, **833**, 155122 (2022). https://doi.org/10.1016/j.scitotenv.2022.155122

[2] Chen L., Luo L., Qin W., Zhu X., Tomberlin J. K., Zhang J., Hou D., Chen H., Yu Z., Zhang Z., Chen D., Li Q.: Recycling nitrogen in livestock wastewater for alternative protein by black soldier fly larvae bioreactor. Environmental Technology Innovation, **29**, 102971 (2023). https://doi.org/10.1016/j.eti.2022.102971

[3] Beyers M., Coudron C., Ravi R., Meers E., Bruun S.: Black soldier fly larvae as an alternative feed source and agro-waste disposal route – A life cycle perspective. Resources, Conservation and Recycling, **192**, 106917 (2023). https://doi.org/10.1016/j.resconrec.2023.106917

[4] Li R., Lin T., Fan X., Dai X., Huang J., Zhang Y., Guo R., Fu S.: Effects of salinity in food waste on the growth of black soldier fly larvae and global warming potential analysis. Chemical Engineering Journal, **480**, 148221 (2024). https://doi.org/10.1016/j.cej.2023.148221

[5] Siddiqui S. A., Ristow B., Rahayu T., Putra N. S., Yuwono N. W., Nisa K., Mategeko B., Smetana S., Saki M., Nawaz A., Nagdalian A.: Black soldier fly larvae (BSFL) and their affinity for organic waste processing. Waste Management, **140**, 1–13 (2022). https://doi.org/10.1016/j.wasman.2021.12.044

[6] Ganesan A. R., Mohan K., Kandasamy S., Surendran R. P., Kumar R., Rajan D. K., Rajarajeswaran J.: Food waste-derived black soldier fly (*Hermetia illucens*) larval resource recovery: A circular bioeconomy approach. Process Safety and Environmental Protection, **184**, 170–189 (2024). https://doi.org/10.1016/j.psep.2024.01.084

[7] Singh A., Kumari K.: An inclusive approach for organic waste treatment and valorisation using black soldier fly larvae: A review. Journal of Environmental Management, **251**, 109569 (2019). https://doi.org/10.1016/j.jenvman.2019.109569

[8] Raksasat R., Lim J. W., Kiatkittipong W., Kiatkittipong K., Ho Y. C., Lam M. K., Font-Palma C., Zaid H. F. M., Cheng C. K.: A review of organic waste enrichment for inducing palatability of black soldier fly larvae: Wastes to valuable resources. Environmental Pollution, **267**, 115488 (2020). https://doi.org/10.1016/j.envpol.2020.115488

[9] Surendra K. C., Tomberlin J. K., van Huis A., Cammack J. A., Heckmann L. H. L., Khanal S. K.: Rethinking organic wastes bioconversion: Evaluating the potential of the black soldier fly (*Hermetia illucens* (L.)) (Diptera: Stratiomyidae) (BSF). Waste Management, **117**, 58–80 (2020). https://doi.org/10.1016/j.wasman.2020.07.050

[10] Mohan K., Rajan D. K., Muralisankar T., Ganesan A. R., Sathishkumar P., Revathi N.: Use of black soldier fly (*Hermetia illucens* L.) larvae meal in aquafeeds for a sustainable aquaculture industry: A review of past and future needs. Aquaculture, **553**, 738095 (2022). https://doi.org/10.1016/j.aquaculture.2022.738095

[11] Meng L., Ma L., Xu J., Rong K., Peng N., Zhao S.: Effect of enzyme-assisted fermentation on quality, safety, and microbial community of black soldier fly larvae (*Hermetia illucens* L.) as a novel protein source. Food Research International, **174**, 113624 (2023). https://doi.org/10.1016/j.foodres.2023.113624

[12] Huseynli L., Parviainen T., Kyllönen T., Aisala H., Vene K.: Exploring the protein content and odor-active compounds of black soldier fly larvae for future food applications. Future Foods, **7**, 100224 (2023). https://doi.org/10.1016/j.fufo.2023.100224

[13] Iñaki G. B. J., Antonio P-C. G., Efrén D., Hiram M-R., Daniela G-I., Damián R-J.: Black soldier fly: Prospection of the inclusion of insect-based ingredients in extruded foods. Food Chemistry Advances, **1**, 100075 (2022). https://doi.org/10.1016/j.focha.2022.100075

[14] Schiavone A., de Marco M. D., Martínez S., Dabbou S., Renna M., Madrid J., Hernandez F., Rotolo L., Costa P., Gai F., Gasco L.: Nutritional value of a partially defatted and a highly defatted black soldier fly larvae (*Hermetia illucens* L.) meal for broiler chickens: Apparent nutrient digestibility, apparent metabolizable energy and apparent ileal amino acid digestibility. Journal of Animal Science and Biotechnology, **8**, 51 (2017). https://doi.org/10.1186/s40104-017-0181-5

[15] Miron L., Montevecchi G., Bruggeman G., Macavei L. I., Maistrello L., Antonelli A., Thomas M.: Functional properties and essential amino acid composition of proteins extracted from black soldier fly larvae reared on canteen leftovers. Innovative Food Science and Emerging Technologies, **87**, 103407 (2023). https://doi.org/10.1016/j.ifset.2023.103407

[16] Abduh M. Y., Perdana M. P., Bara M. A., Anggraeni L. W., Putra R. E.: Effects of aeration rate and feed on growth, productivity and nutrient composition of black soldier fly (*Hermetia illucens* L.) larvae. Journal of Asia-Pacific Entomology, **7**, 101902 (2022). https://doi.org/10.1016/j.aspen.2022.101902

[17] Krishnan S., Paul P. K., Rodriguez T. A.: Cell competition and the regulation of protein homeostasis. Current Opinion in Cell Biology, **87**, 102323 (2024). https://doi.org/10.1016/j.ceb.2024.102323

[18] Bouwstra J. A., Helder R. W. J., El Ghalbzouri A.: Human skin equivalents: Impaired barrier function in relation to the lipid and protein properties of the stratum corneum. Advanced Drug Delivery Reviews, **175**, 113802 (2021). https://doi.org/10.1016/j.addr.2021.05.012

[19] Dehnad D., Ghorani B., Emadzadeh B., Zhang F., Yang N., Jafari S. M.: Electrospinning of legume proteins: Fundamentals, fiber production, characterization, and applications with a focus on soy proteins. Food Hydrocolloids, **151**, 109795 (2024). https://doi.org/10.1016/j.foodhyd.2024.109795

[20] Pires J. B., dos Santos F. N., de Lima Costa I. H., Kringel D. H., da Rosa Zavareze E., Dias A. R. G.: Essential oil encapsulation by electrospinning and electrospraying using food proteins: A review. Food Research International, **170**, 112970 (2023). https://doi.org/10.1016/j.foodres.2023.112970

[21] Syed M. H., Khan M. M. R., Zahari M. A. K. M., Beg M. D. H., Abdullah N.: Current issues and potential solutions for the electrospinning of major polysaccharides and proteins: A review. International Journal of Biological Macromolecules, **253**, 126735 (2023). https://doi.org/10.1016/j.ijbiomac.2023.126735

[22] Xie S., Hu J., Li K., Zhao Y., Ma N., Wang Y., Jin Y., Guo G., Kumar R., Li J., Huang J., Tian H.: Substantial and efficient adsorption of heavy metal ions based on protein and polyvinyl alcohol nanofibers by electrospinning. International Journal of Biological Macromolecules, **253**, 126536 (2024). https://doi.org/10.1016/j.ijbiomac.2023.126536

[23] Zhao X., Han Z., Zhang S., Abuduaini G., Wen X., Liu T., Cheng Z.: Preparation of PVA/*Tremella* polysaccharide and soy protein isolate complex/ε-polylysine active membrane and its application in blueberry preservation. Food Packaging and Shelf Life, **40**, 101163 (2023). https://doi.org/10.1016/j.fpsl.2023.101163

[24] Rostami M., Beheshtizadeh N., Ranjbar F. E., Najafi N., Ahmadi A., Ahmadi P., Rostamabadi H., Pazhouhnia Z., Assadpour E., Mirzanajafi-Zanjan M., Kisomi M. F., Kharazmi M. S., Jafari S. M.: Recent advances in electrospun protein fibers/nanofibers for the food and biomedical applications. Advances in Colloid and Interface Science, **311**, 102827 (2023). https://doi.org/10.1016/j.cis.2022.102827

[25] Ghomi E. R., Khosravi F., Neisiany R. E., Shakiba M., Zare M., Lakshminarayanan R., Chellappan V., Abdouss M., Ramakrishna S.: Advances in electrospinning of aligned nanofiber scaffolds used for wound dressings. Current Opinion in Biomedical Engineering, **22**, 100393 (2022). https://doi.org/10.1016/j.cobme.2022.100393

[26] Mohammadalizadeh Z., Bahremandi-Toloue E., Karbasi S.: Recent advances in modification strategies of pre- and post-electrospinning of nanofiber scaffolds in tissue engineering. Reactive and Functional Polymers, **172**, 105202 (2022). https://doi.org/10.1016/j.reactfunctpolym.2022.105202

[27] Suarato G., Contardi M., Perotto G., Heredia-Guerrero J. A., Fiorentini F., Ceseracciu L., Pignatelli C., Debellis D., Bertorelli R., Athanassiou A.: From fabric to tissue: Recovered wool keratin/polyvinylpyrrolidone biocomposite fibers as artificial scaffold platform. Materials Science and Engineering C, **116**, 111151 (2020). https://doi.org/10.1016/j.msec.2020.111151

[28] Flores-Nieves M. M., Castellanos-Espinoza R., Estevez M., Baldenegro-Pérez L. A., Trejo J. F. G., García M. E., Cano B. M., Soto-Zarazúa G. M., España-Sánchez B. L.: Electrospun casein fibers obtained from revalued milk with mechanical and antibacterial properties. Arabian Journal of Chemistry, **15**, 104201 (2022). https://doi.org/10.1016/j.arabjc.2022.104201

[29] Salehi A. O. M., Keshel S. H., Sefat F., Tayebi L.: Use of polycaprolactone in corneal tissue engineering: A review. Materials Today Communications, **27**, 102402 (2021). https://doi.org/10.1016/j.mtcomm.2021.102402

[30] Bartnikowski M., Dargaville T. R., Ivanovski S., Hutmache D. W.: Degradation mechanisms of polycaprolactone in the context of chemistry, geometry and environment. Progress in Polymer Science, **96**, 1–20 (2019). https://doi.org/10.1016/j.progpolymsci.2019.05.004

[31] Kumawat V. S., Saini R. K., Agrawal A. K., Khare D., Dubey A. K., Ghosh S. B., Bandyopadhyay-Ghosh S.: Nano-fluorcanasite-fluorapatite reinforced poly-ε-caprolactone based biomimetic scaffold: A synergistic approach towards generation of conducive environment for cell survival. Journal of Polymers and the Environment, **32**, 411–429 (2023). https://doi.org/10.1007/s10924-023-02977-w

[32] Kumawat V. K., Bandyopadhyay-Ghosh S., Ghosh S. B.: An overview of translational research in bone graft biomaterials. Journal of Biomaterials Science, Polymer Edition, **34**, 497–540 (2023). https://doi.org/10.1080/09205063.2022.2127143

[33] Wu C-S.: Interface design, cytocompatibility, and biological activity of astaxanthin/polyester composites. International Journal of Polymeric Materials and Polymeric Biomaterials, **67**, 564–571 (2018). https://doi.org/10.1080/00914037.2017.1354203

[34] Yao Y., Zhang X., Guo Z., Liu W., Hu C., Ru Y., Zhang L., Jiang C., Qiao J.: Preparation and application of recyclable polymer aerogels from styrene-maleic anhydride alternating copolymers. Chemical Engineering Journal, **455**, 140363 (2023). https://doi.org/10.1016/j.cej.2022.140363

[35] Zhang F., Xu Y., Kong B., Chen Q., Sun F., Zhang H., Liu Q.: Comparative study of two types of pre-extraction treatment (drying or non-drying) on physicochemical, structural and functional properties of extracted insect proteins from *Tenebrio molitor* larvae. Current Research in Food Science, **5**, 1570–1580 (2022). https://doi.org/10.1016/j.crfs.2022.09.004

[36] Wu C-S.: Influence of modified polyester on the material properties of collagen-based biocomposites and *in vitro* evaluation of cytocompatibility. Materials Science and Engineering C, **48**, 310-319 (2015). https://doi.org/10.1016/j.msec.2014.12.013

[37] Shih Y-F., Chou M-Y., Chang W-C., Lian H-Y., Chen C-M.: Completely biodegradable composites reinforced by the cellulose nanofibers of pineapple leaves modified by eco-friendly methods. Journal of Polymers Research, **24**, 209 (2017). https://doi.org/10.1007/s10965-017-1367-4

[38] Lin Y., Ou Y., Xu M., Chen J.: Enhancing bone regeneration with bionic hydrolysis and biomimetic polydopamine coating on 3D-printed PCL scaffolds: A comparative study. Materials Today Communications, **37**, 107262 (2023). https://doi.org/10.1016/j.mtcomm.2023.107262

[39] Zhou L., He H., Li M-C., Huang S., Mei C., Wu Q.: Enhancing mechanical properties of poly(lactic acid) through its *in-situ* crosslinking with maleic anhydride-modified cellulose nanocrystals from cottonseed hulls. Industrial Crops and Products, **112**, 449-459 (2018). https://doi.org/10.1016/j.indcrop.2017.12.044

[40] Wu X., Zhao W., Wang X., Bai Z., Ma L.: A novel variable power microwave (VPM) drying technology for lowering energy consumption and improving the *in vitro* protein digestibility of black solider fly larvae. Innovative Food Science and Emerging Technologies, **89**, 103470 (2023).
https://doi.org/10.1016/j.ifset.2023.103470

[41] Gautam S., Purohit S. D., Singh H., Dinda A. K., Potdar P. D., Sharma C., Chou C-F., Mishra N. C.: Surface modification of PCL-gelatin-chitosan electrospun scaffold by nano-hydroxyapatite for bone tissue engineering. Materials Today Communications, **34**, 105237 (2023).
https://doi.org/10.1016/j.mtcomm.2022.105237

[42] Liu C., Wang C., Yao H., Chapman S. J.: Pretreatment is an important method for increasing the conversion efficiency of rice straw by black soldier fly larvae based on the function of gut microorganisms. Science of the Total Environment, **762**, 144118 (2021).
https://doi.org/10.1016/j.scitotenv.2020.144118

[43] Wu C-S., Wu D-Y., Wang S-S.: Nanocomposites of biobase polyester containing natural hydroxyapatite and duck eggshell made by electrospinning: Fabrication and characterization. Journal of Polymers and the Environment, **31**, 519–532 (2023).
https://doi.org/10.1007/s10924-022-02558-3

[44] Pan J., Xu H., Dabbour M., Mintah B. K., Huang L., Dai C., He R., Ma H.: Effect of pectin concentration on emulsifying properties of black soldier fly (*Hermetia illucens*) larvae albumin modified by pH-shifting and ultrasonication. International Journal of Biological Macromolecules, **257**, 128779 (2024).
https://doi.org/10.1016/j.ijbiomac.2023.128779

[45] Lu S., Taethaisong N., Meethip W., Surakhunthod J., Sinpru B., Sroichak T., Archa P., Thongpea S., Paengkoum S., Purba R. A. P., Paengkoum P.: Nutritional composition of black soldier fly larvae (*Hermetia illucens* L.) and its potential uses as alternative protein sources in animal diets: A review. Insects, **13**, 831 (2022).
https://doi.org/10.3390/insects13090831

[46] Dolatabadi E. N., Asghariazar V., Darvish M., Nejati-Koshki K.: Simvastatin-loaded PCL/PEG nanofibrous scaffold: A prospective approach for suppression 5-fluorouracil resistance in MKN-45 gastric cancer cells. Journal of Drug Delivery Science and Technology, **80**, 104104 (2023).
https://doi.org/10.1016/j.jddst.2022.104104

[47] Montevecchi G., Licciardello F., Masino F., Miron L. T., Antonelli A.: Fortification of wheat flour with black soldier fly prepupae. Evaluation of technological and nutritional parameters of the intermediate doughs and final baked products. Innovative Food Science and Emerging Technologies, **69**, 102666 (2021).
https://doi.org/10.1016/j.ifset.2021.102666

[48] Caligiani A., Marseglia A., Leni G., Baldassarre S., Maistrello L., Dossena A., Sforza S.: Composition of black soldier fly prepupae and systematic approaches for extraction and fractionation of proteins, lipids and chitin. Food Research International, **105**, 812–820 (2018).
https://doi.org/10.1016/j.foodres.2017.12.012

[49] Van J. C. F., Tham P. E., Lim H. R., Khoo K. S., Chang J-S., Show P. L.: Integration of internet-of-things as sustainable smart farming technology for the rearing of black soldier fly to mitigate food waste. Journal of the Taiwan Institute of Chemical Engineers, **137**, 10423 (2022).
https://doi.org/10.1016/j.jtice.2022.104235